Advantages of the unscavenged pre-chamber ignition system in turbocharged natural gas engines for automotive applications

J. J. López[a], R. Novella[a], J. Gomez-Soriano[a,*], P. J. Martinez-Hernandiz[a], F. Rampanarivo[b], C. Libert[b], M. Dabiri[b]

[a]*CMT – Motores Térmicos, Universitat Politècnica de València, Camino de Vera, 46022 Valencia, Spain*
[b]*DEA-IRP Groupe Renault, 1 avenue du Golf. 78084, Guyancourt, France*

Abstract

In view of the increasing restrictions for CO_2 mitigation, the evaluation of alternative fuels to ensure sustainability of transportation is becoming increasingly important. Since some of these alternatives can be refined from renewable sources, they are interesting from the perspective of both: the use of the current power-plants and the CO_2 emission. In this sense, natural gas arises as an interesting propellant to substitute fossil fuels. Therefore, combining this fuel with specific combustion strategies can help to decrease the environmental footprint of transportation in the broadest sense. In this paper, an evaluation of the possible advantages of this combination has been conducted. The investigation has been carried out in a port fueled turbocharged spark-ignition engine, using compressed natural gas (CNG) and a passive pre-chamber ignition system. The effects of the CNG fuel properties on combustion have been analyzed and the global impact of using CNG for transportation has been appraised by means of the life cycle assessment. Results show that combustion of CNG refined by different renewable sources not only reduces the global CO_2 emission but also can contribute to remove the existent pollution. In addition, they show an increase of the engine thermal efficiency when combining CNG and the pre-chamber ignition concept.

Keywords: *Natural Gas SI Engine, Pre-chamber Ignition, Lean Burn, EGR-diluted combustion, LCA*

1. Introduction

Nowadays, one of the most challenging problems that humans are facing is the global climate change. Temperatures around the world, specially in the marine biomes [1, 2], are increasing and their future consequences are still unknown. This climate change is mainly motivated by the human activity, being industry, transportation and power generation the main contributors. The usual work of these activities generate a series of greenhouse gases (GHG), among them, carbon dioxide (CO_2) and nitrogen oxides (NO_x) and other hazardous pollutants such as particulate matter (PM) [3].

In order to mitigate the effects of this gaseous waste, leaders of many countries have signed agreements to reduce their emissions (Paris Agreement or Kyoto Protocol). In this way, future prospects have been performed in different regions, whereas numerous studies to accomplish the proposed objectives have been carried out [4, 5, 6]. In all these studies, the global impact of the fuel (or the life cycle of the fuel production) utilization is assessed by considering two main contributions: the GHG emission produced as the fuel is consumed in the vehicle (tank-to-wheel) and also as the fuel travels from the extraction to the refueling station (well-to-tank).

One of the most popular solutions to reduce GHG in transportation is the shifting from internal combustion engines (ICE) to complete electric engines (EV). Although this is a straightforward solution and the current electric engine technology allowed this migration, other issues related to the energy storage should still be addressed. The basic infrastructure to recharge batteries is not fully developed in most places. Therefore, other short-term solutions should be considered in other to mitigate the overall GHG emission. For instance, the use of fuels that can be refined from renewable sources (i.e. compressed natural gas (CNG) [7, 8]) are interesting in terms of both the current ICE technology and the GHG emission as well.

Previous life cycle assessments (LCA) carried out to quantify the benefit of using natural gas [9] refined by following an European mix prospect of different sources [10] (i.e. landfill gas or food waste), showed that the overall estimated GHG emission resulting from combustion is clearly reduced if it is compared to traditional gasoline-based fuels. The organic waste from human activities can be also recycled and turned into gaseous fuels to employ them in transportation power-plants. This contributes to a circular economy [11] that minimizes the use of resources by creating closed-loops of processes with an evident benefit for the planet. If this waste recycling is combined with combustion strategies that enhance the overall efficiency of the engines (reducing pollutant emissions and the fuel consumption), the benefits of CNG combustion are even more evident [12].

*Corresponding author.
Tel.: +34 96 387 70 00 (ext. 76537), fax: +34 96 387 76 59
email: jogoso1@mot.upv.es

One of these strategies is the lean combustion [13], which consists in diluting the air-fuel mixture, with air and/or recirculated exhaust gases (EGR). This increased dilution leads to a reduced pumping losses [14], a lower heat loss through the chamber walls and an increase in the specific heat ratio. In this way, an improved thermal efficiency [15, 16] can be achieved.

In these conditions, the charge ignition and the combustion stability is compromised [17], thus a source that provides an increased ignition energy is mandatory to assure the viability of lean combustion [18, 19]. Several technologies based on increasing ignition energy deposition have been developed during the last decade. Among them, the pre-chamber ignition system, commercially known as Turbulent Jet Ignition (TJI) [20, 21], seems an interesting solution to extend the current limits of lean combustion (ignition issues and combustion stability). The higher burning rates generated by the TJI concept [22] leads to additional advantages such as enhanced combustion phasing and combustion stability (a reduced cycle-to-cycle variability is achieved), that subsequently improves the engine thermal efficiency [23]. However, the pre-chamber scavenge and the increased heat transfer at low load/speed engine conditions are some of the main drawbacks identified to date [24].

There are two different pre-chamber ignition concept approaches: active and passive (or unscavenged). The mechanical simplicity of the passive system, which has no additional fuel supply within the pre-chamber, makes its implementation an interesting solution due to packaging and assembly costs

The application of natural gas in large engines has been previously investigated by Mastorakos et al. [25]. Other authors [26, 27, 28, 29] demonstrated that using CNG fuel could be an interesting application for stationary engines and for heavy-duty engines [30, 31, 32, 33]. Therefore, in combination with the TJI concept and other strategies to reduce pollutant emissions [34], the use of natural gas for automotive applications is an interesting strategy to explore since the global impact of the energy utilization is reduced by two fronts: the well-to-tank and also the tank-to-wheel contributions [35, 36].

The investigation conducted in this paper focuses on increasing thermal efficiency while decreasing, or at least keeping, pollutant emission levels of the future generation of natural gas SI engines, thereby contributing to decrease the environmental footprint of the transportation sector.

2. Experimental and numerical setups

2.1. Engine architecture and test cell characteristics

The experimental campaign was developed in a 4-stroke turbocharged spark-ignition research engine used in previous investigations [24, 37]. In this case, the engine compression ratio has increased up to 13.4. The engine specifications and some geometrical features are presented in Table 1 and Fig. 1 for reference.

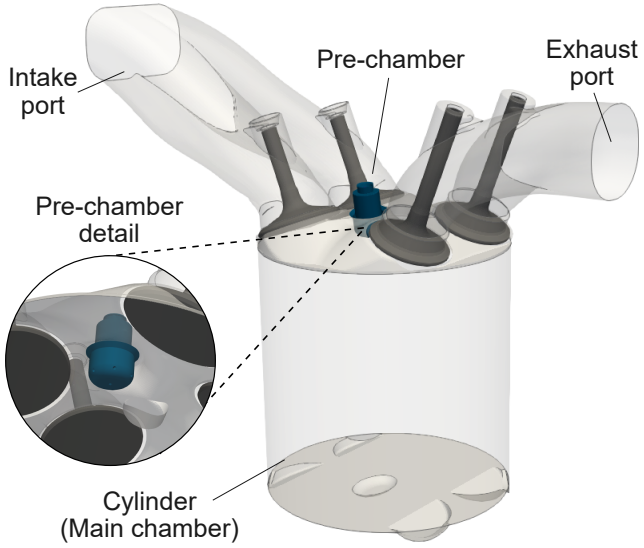

Figure 1: *Outline of the pre-chamber and combustion chamber design including the intake and exhaust ports geometry.*

Table 1: *Engine specifications.*

Engine	**4-stroke research SI**
Cylinders [-]	1
Bore [mm]	80.0
Stroke [mm]	80.5
Displacement [cm^3]	404
Compression ratio (geometric) [-]	13.4:1
Valvetrain [-]	DOHC
Number of valves/cylinder [-]	4
Fuel injection system [-]	PFI (P_{max} = 6 bar)

The test cell layout in which the engine is assembled, is presented in Figure 2. This installation shares the main equipment shown in previous works [24, 37]. However, some modifications related to the fuel injection system were performed to deal with the compressed natural gas properties. The instantaneous fuel consumption was measured by a BRONKHORST F-113AC-M50-AAD-44-V flowmeter. The main features of the fuel are summarized in Table 2. The fuel is supplied in the intake manifold 270 mm away from cylinder head using a PFI gas system to avoid mixture heterogeneities.

Table 2: *Main specifications of the fuel.*

Type	**CNG**
RON	120
A/F_{st}	16.72
Lower Heating Value (LHV)	48.931 MJ/kg
Density (15°C)	5 kg/m^3
H/C ratio	3.84 mol/mol
O/C ratio	0.0 mol/mol
Oxygen content	0.0 %
Reduced formula ($C_xH_yO_z$)	1.077 (x) - 4.137 (y) - 0.0 (z)

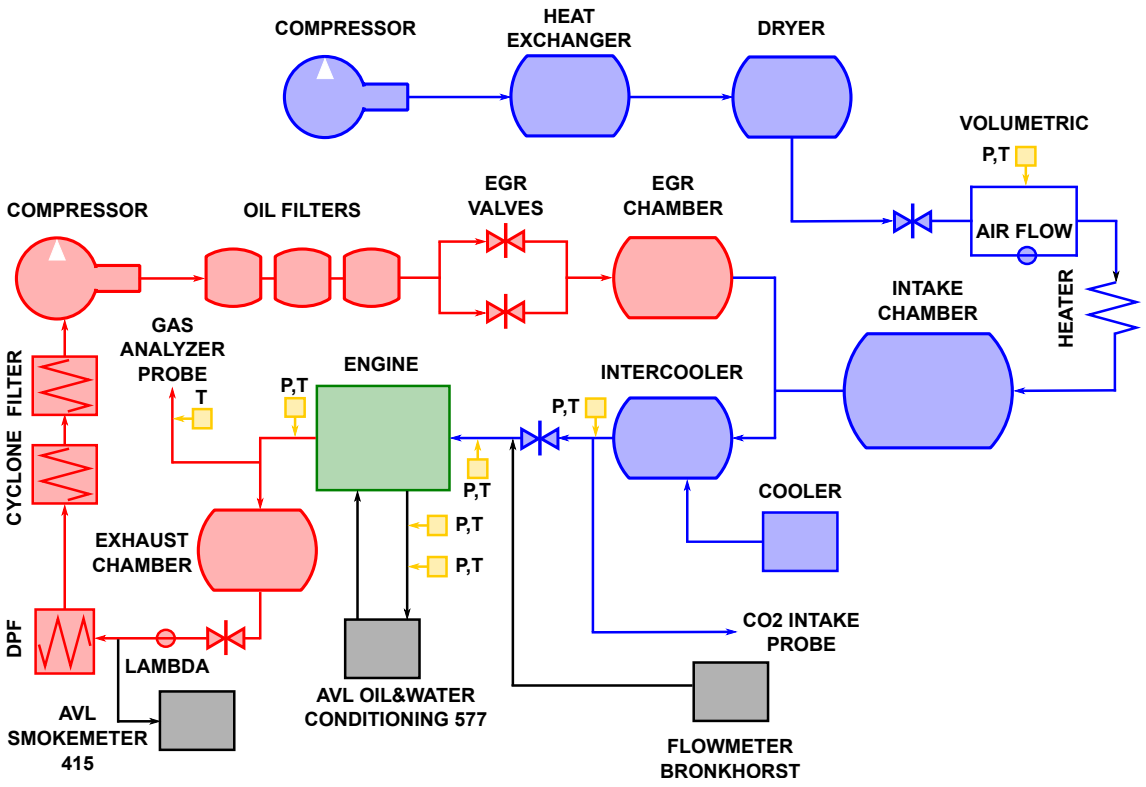

Figure 2: *Layout of the engine test cell.*

2.2. *Modeling tools*

A numerical tool based on a 1D Wave Action Model (WAM) is used in this investigation. The original model, which contains the layout of the test bench and the referred engine, was developed in the author's previous work [24]. However, it was improved in this investigation by adding a modal node temperature layout for the pre-chamber using the existent functionalities of the 1D simulation software. With this modification, the model allows an improved prediction of the heat transferred through the pre-chamber walls. In this sense, the temporal evolution of the pre-chamber walls temperature is obtained after an iterative procedure.

Results of both models (the original, defined in [24], and the improved one) are compared against experiments coming from the test bench in Fig. 3. Although this procedure was also performed for the two operating conditions (described in Table 3), only a validation for medium engine load (6.8 bar IMEP) and speed (2000 rpm) is shown for simplicity. As shown in this figure, the new model formulation helps to better capture the experiment trends. The improved prediction of the pressure difference between both chambers allows an accurate estimation of the maximum in-cylinder pressure, providing reliable information for further analysis.

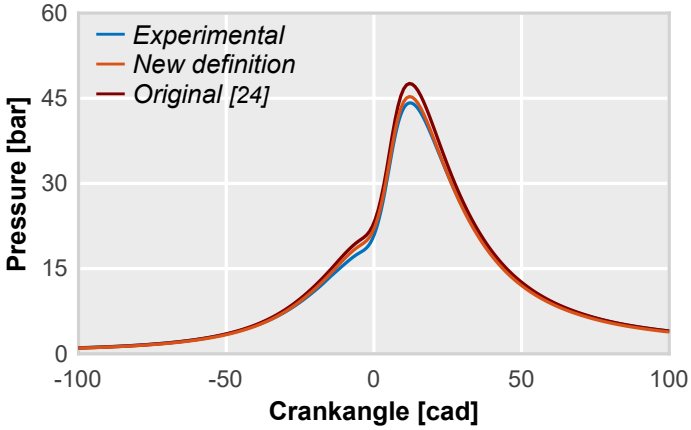

Figure 3: *Validation of the 1D WAM model. Comparison of in-cylinder pressure profiles.*

3. Methodology

An experimental campaign was performed to compare the engine performance and emissions levels of the conventional spark-ignition concept against the two passive pre-chamber geometries. The main geometrical characteristics of the pre-chambers are shown in Table 3 and Fig. 4. Since none of them have additional fuel supply inside the pre-chamber unit, the fuel is provided by the compression effect of the piston. The differences among them are focused on the volume (keeping the internal diameter and modifying its length) and the number of nozzles. Both pre-chamber designs were specifically optimized for operating with gasoline fuel [24]. As will be seen below, this fact will have significant effects on the results. The target IMEP was obtained by sweeping the spark timing till achieving the MBT at stoichiometric condi-

tions with no EGR. Once this fuel amount was obtained, it was maintained for the remaining tests at the same engine speed and load conditions. For the spark timing sweep tests, the procedure was the same but 3 to 5 points were measured advancing and delaying the spark timing in 2 cad intervals from the MBT.

Table 3: *Pre-chamber geometrical parameters.*

Pre-chamber	PC1	PC2
Normalized volume [-]	1	0.6
Normalized diameter [-]	1	1
Number of holes [-]	6	4

The operating conditions selected to conduct the experimental campaign were specifically chosen to gather the most critical conditions from the point of view of the pre-chamber scavenge and filling. The first point investigated has been widely studied in the author's previous work [24], and it consists in a combination of medium-to-high engine speed (4500 rpm) and medium-to-high engine load (12.8 bar IMEP) (OP1). This operating condition compromises the scavenging of the pre-chamber, being a critical aspect in this kind of ignition systems. Besides, this engine load causes the appearance of knock events that should be investigated.

The second point corresponds with the combination of low engine speed (1350 rpm) and low engine load (2.8 bar IMEP) (OP2) at cold conditions (oil and water temperatures at 90ºC). This point is interesting since the fuel amount into the pre-chamber is limited by the low engine load, and the operation of the concept itself could be compromised.

After defining the target operating conditions, this research work follows a logical chronology. Starting from the high speed/load point and finishing with the low speed/load operating point.

For the highest engine load point, the three ignition systems (conventional SI and both pre-chamber definitions) were also evaluated in diluted conditions, by increasing the relative air-to-fuel ratio (λ) in steps of 0.2 and the EGR rate in steps of 10%. The limit set for the maximum dilution ratio was imposed by the combustion stability, with a maximum stable value of IMEP CoV 10%.

The final stage of the experimental testing plan consisted in several activities regarding the low engine load operating condition. For this point, a spark timing sweep was performed initially by increasing EGR dilution level and later by increasing intake temperature. The purpose of these activities is to try to increase the exhaust temperature compared to the conventional spark-ignition concept. Performed activities are summarized in Table 4, showing the maximum dilution ratio achieved, for both λ and EGR.

Table 4: *Operating settings for the experimental campaign.*

		OP1	**OP2**
Engine speed [rpm]		4500	1350
IMEP [bar]		12.8	2.8
SI	λ	1.0 : 0.2 : 1.6	1.0
	EGR [%]	0 : 10 : 30	0 : 5 : 10
	ST [cad]	MBT	Sweep + Int. Temp.
PC1	λ	1.0 : 0.2 : 1.55	1.0
	EGR [%]	0 : 10 : 25	0 : 5 : 10
	ST [cad]	MBT	Sweep + Int. Temp.
PC2	λ	1.0 : 0.2 : 1.45	1.0
	EGR [%]	0 : 10 : 22	0
	ST [cad]	MBT	Sweep

4. Results and discussion

4.1. Preliminary fuel study

Despite the fact that natural gas is a promising alternative to conventional gasoline, it must be kept in mind that there are some substantial differences between both fuels. As these differences affect the thermochemical properties of the mixture, the combustion process can be strongly conditioned, especially in terms of burning rate and knock onset by the end-gas auto-ignition. Since both phenomena entail intricate turbulence interactions and spatio-temporal thermodynamic interplays, their assessment is not simple and usually requires complex and high computational resources. Nevertheless, the analysis of the pure thermochemical properties of the fuel could shed some light on what we could expect when changing from conventional gasoline to CNG fuel. In tis way, more simplistic simulations based on the laminar flame properties and the chemical auto-ignition can be used.

In order to analyze the impact in the laminar properties of the flame, a preliminary modeling activity was carried out. Assuming the same gross IMEP target, the same gross indicated efficiency and controlling the air flow by the intake pressure, the expected air flow rates for both fuels were calculated. It was considered that regular gasoline has an stoichiometric air-to-fuel ratio (A/F_{stoich}) of 14.37 whereas CNG fuel has 16.72. The LHV of the gasoline is 42.793 MJ/kg and the LHV of the compressed natural gas is 48.931 MJ/kg. The expected air flow increment necessary to keep the same gross IMEP operating with compressed natural gas is around 2-3%, so the pressure should increase in the same range.

Assuming that this increment in the intake pressure is negligible, the sensibility of both fuels to the laminar flame speed was calculated by means of a 1D flame speed model [38]. In this study, the intake temperature, pressure, λ and EGR were varied. Results of this calculation are presented in Fig. 5, in which the difference between the laminar flame speeds of gasoline and natural gas is plotted. The fixed variables of these graphs were estimated from the experimental data at the spark time of the first operation point (OP1).

In this figure a positive value indicates that natural gas flame speed is lower than gasoline flame speed. Results show how the natural gas laminar flame speed is lower than that

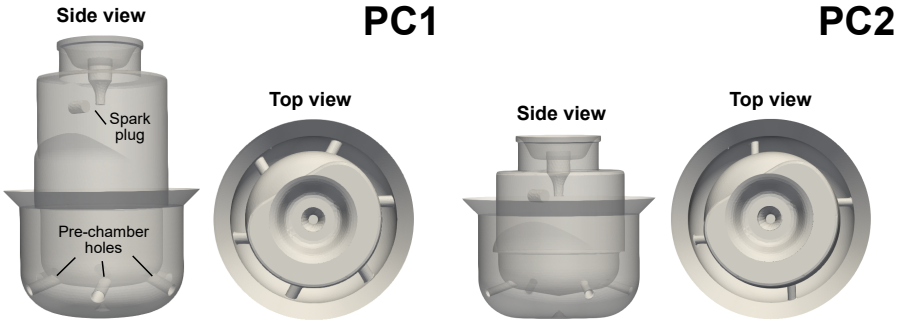

Figure 4: *Sketch of pre-chamber geometries (PC1 and PC2).*

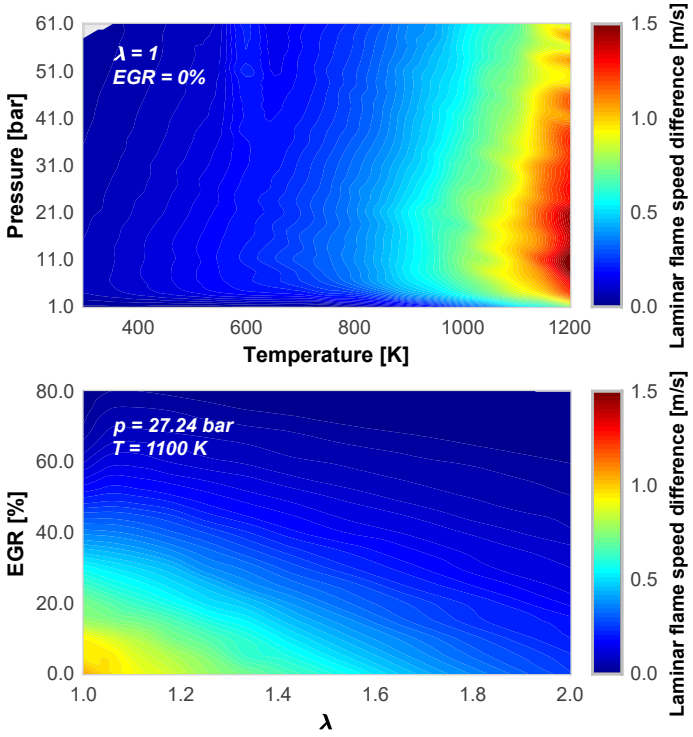

Figure 5: *Difference in laminar flame speed for gasoline and compressed natural gas at different pressure, temperature, λ and EGR levels.*

of the gasoline fuel in all conditions since there are no values below zero. Examination of the top graph reveals that an increase in the pressure has small effect in flame speed, while it is also seen that increasing temperatures tend to rise the gap between both fuels. Regarding the sensitivity to λ and EGR, similar trends are observed: an increase in the dilution ratio reduces the gap between both fuels.

In Fig. 6 the auto-ignition delay (τ) is plotted against temperature and air dilution ratio. The objective is to locate the most interesting operating condition point studied in gasoline [24] and to compare the knock propensity when changing fuel. A representative combustion duration (CD) without knock limitation (obtained from the experimental database) is plotted as a black line, while the high load/speed operation condition is pointed in the map. Shaded regions correspond to the situations where the auto-ignition delay does not exceed the representative CD, that is when knocking combustion could appear. The pressure considered coincides with the value at which the 50% of the fuel is burned (CA50). This value should be representative of the average pressure inside the chamber when end-gas knock appears.

In this figure, the negative temperature coefficient (NTC) region, which is associated with the primary dissociation of the iso-octane chains [39, 40], is observed for gasoline whereas it is not present in the CNG map. In addition to this, the benefits of using CNG are evident when comparing both shaded regions (gasoline vs. CNG). While the operating range is extremely narrow in the gasoline fuel map, the auto-ignition delay increases almost three orders of magnitude if CNG is used as fuel, thus hindering the knock onset appearance in most of the simulated conditions. For instance, comparing the stoichiometric simulation ($\lambda = 1$ no EGR) highlighted in both maps and performed at 860K and 30.86 bar, it can be seen how τ increases from 0.41 to 100.75 ms.

This notable increment of the auto-ignition delay makes the concept itself more flexible since a suitable combustion phasing can be reached without any risk of knock issues. In addition, since the laminar flame speed of natural gas is worse compared to the gasoline fuel, parallel actions must be taken to compensate the burning rate lowering. For example, in the hypothetical case that the burning rate could be maintained between both fuels (by increasing the turbulence contribution), the benefits in knock tolerance should be evident.

4.2. Life cycle assessment

In order to estimate the global impact on the GHG emission when switching to compressed natural gas fuel, a life cycle analysis has been carried out using the GREET software developed by Argonne National Laboratories [41]. This software provides an general outlook of pollutant emissions generated in the whole production, transportation and compression process of different fuels. The European mix of renewable natural gas production [10] is considered being a combination of food waste (74%), landfill gas (17%) and waste sludge (9%) processes. The life cycle analysis shown in Table 5, shows a comparison of the pollutant emissions between conventional natural gas (NG), natural gas coming

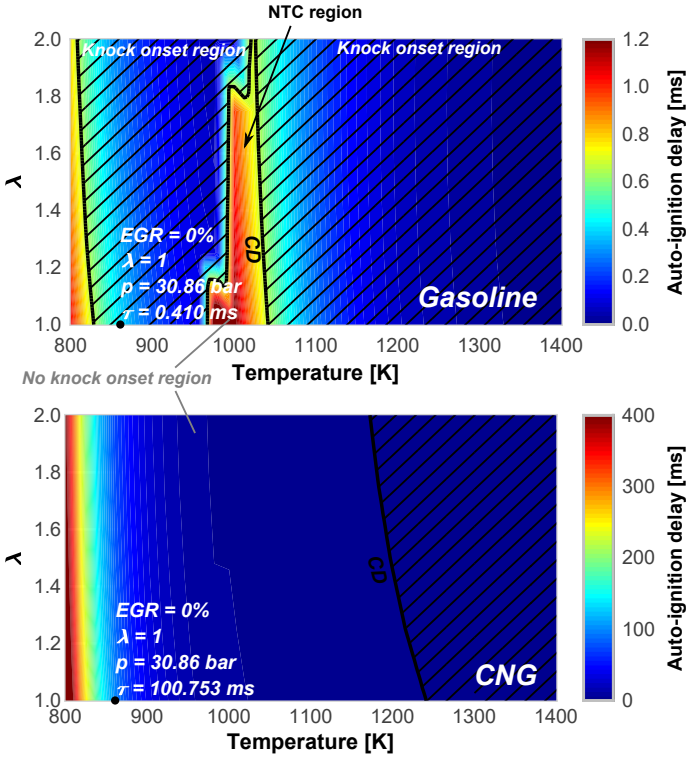

Figure 6: *Auto-ignition delay calculated for gasoline (top) and compressed natural gas (bottom). Black lines represent the combustion duration without knock limitation (CD).*

from food waste (FW), natural gas coming from landfill gas recovery (LG), natural gas coming from waste sludge (WS) and gasoline with 10% of ethanol. The composition of the natural gas is compatible with a CNG refined from different renewable sources.

Focusing on the GHG emission, results of the life cycle assessment show a clear reduction when switching from gasoline to of natural gas. For instance, comparing gasoline and conventional natural gas, the overall emission in 100 years is 2.18E-2 kg/MJ and 1.57E-2 kg/MJ respectively. In addition, using natural gas refined by renewable sources decrease the values below zero, which means that GHG present in the atmosphere are being consumed. In this way, the use of natural gas coming from renewable sources could contribute to stabilize climate change by removal of CO_2 [42] and other GHG. Thus, the interest of developing new combustion strategies that help to reduce the fuel consumption when using renewable-based source fuels is clear and they will enable the future application of these new technologies.

4.3. The passive pre-chamber ignition concept in diluted conditions

As previously reported [24], the TJI concept significantly improves the gross indicated efficiency at high load/speed conditions when knocking combustion is the main limitation to achieve MBT. The improvement of this efficiency is related to the better combustion phasing as a result of the increased combustion rate.

Table 5: *Life cycle assessment of natural gas and gasoline E10.*

Emissions (kg per MJ of fuel) Well to Use					
	NG	FW	LG	WS	Petrol E10
CO_2	7.88E-3	3.54E-2	-5.51E-2	-5.27E-2	1.78E-2
VOC	1.05E-5	-3.21E-5	-2.61E-5	-1.10E-4	2.80E-5
CO	3.51E-5	-2.40E-5	-3.63E-5	-1.24E-4	1.68E-5
NO_x	4.28E-5	-7.82E-6	-9.23E-6	-1.57E-4	3.25E-5
PM_{10}	1.54E-6	-5.02E-6	-4.08E-6	-4.52E-5	3.68E-6
$PM_{2.5}$	7.69E-7	-4.89E-6	-4.77E-6	-3.06E-5	2.32E-6
SO_x	1.49E-5	-6.73E-5	3.80E-6	-1.05E-3	1.48E-5
CH_4	2.43E-4	-5.27E-3	3.73E-4	-7.12E-4	1.09E-4
N_2O	1.53E-6	-5.77E-6	-1.08E-6	-2.31E-5	2.40E-6
BC	1.72E-7	-3.64E-6	-5.36E-6	-6.66E-6	3.43E-7
POC	2.46E-7	6.06E-7	2.11E-7	-1.74E-6	5.74E-7
GHG-100	1.57E-2	-1.24E-1	-4.43E-2	-8.07E-2	2.18E-2

In Fig. 7, the measured in-cylinder pressure and the estimated rate of heat release profiles for SI and TJI (with both considered pre-chambers) at stoichiometric conditions are plotted. The averaged cycle is included together with the standard deviation to account for the cycle-to-cycle variability (CCV). An increment in the maximum pressure (around 20%) is observed when switching from spark-ignition to TJI concept. This is caused by the higher heat release rate provided by the pre-chamber concept. The combustion phasing is also shifted closer to TDC (i.e. coming from 9 to 5 cad aTDC in the PC1 configuration). In contrast to what observed when operating with low RON fuels such as gasoline (RON98) [24], the characteristic rise in the heat release trace during the expansion stroke due to the end-gas auto-ignition is not observed. In terms of fuel admission inside the pre-chamber, it is achieved due to the piston compression. Piston motion forces the air-fuel mixture in the main chamber to enter into the pre-chamber through the holes.

Examination of Fig. 8 corroborates that knock is not a limiting factor using a compressed natural gas (RON120) fuel, even in the case of conventional SI. Note that none of the measured points exceed the knock limit (1 bar). Thus, MBT conditions can be achieved in any of the combustion concepts used. In this situation, where the combustion phasing can be optimized without any relevant restriction, the efficiency gain between conventional SI and TJI is negligible. This is in line with the trends observed in previous research works [24] for lower engine loads.

In Fig. 9, the trends when increasing the air dilution ratio are presented. The most relevant engine outputs for conventional SI and both TJI pre-chambers are plotted against the λ value. Results reproduce the well-known trends as the air-to-fuel ratio is increased. The gross indicated efficiency progressively increases until the maximum dilution level is reached. In all cases, this point is followed by a sharp drop in efficiency mostly caused by the substantial increment of the cycle-to-cycle dispersion. This is clearly reflected in the increase in the coefficient of variation (COV) of IMEP, but also in the combustion efficiency decline. For example, focusing on PC1, the

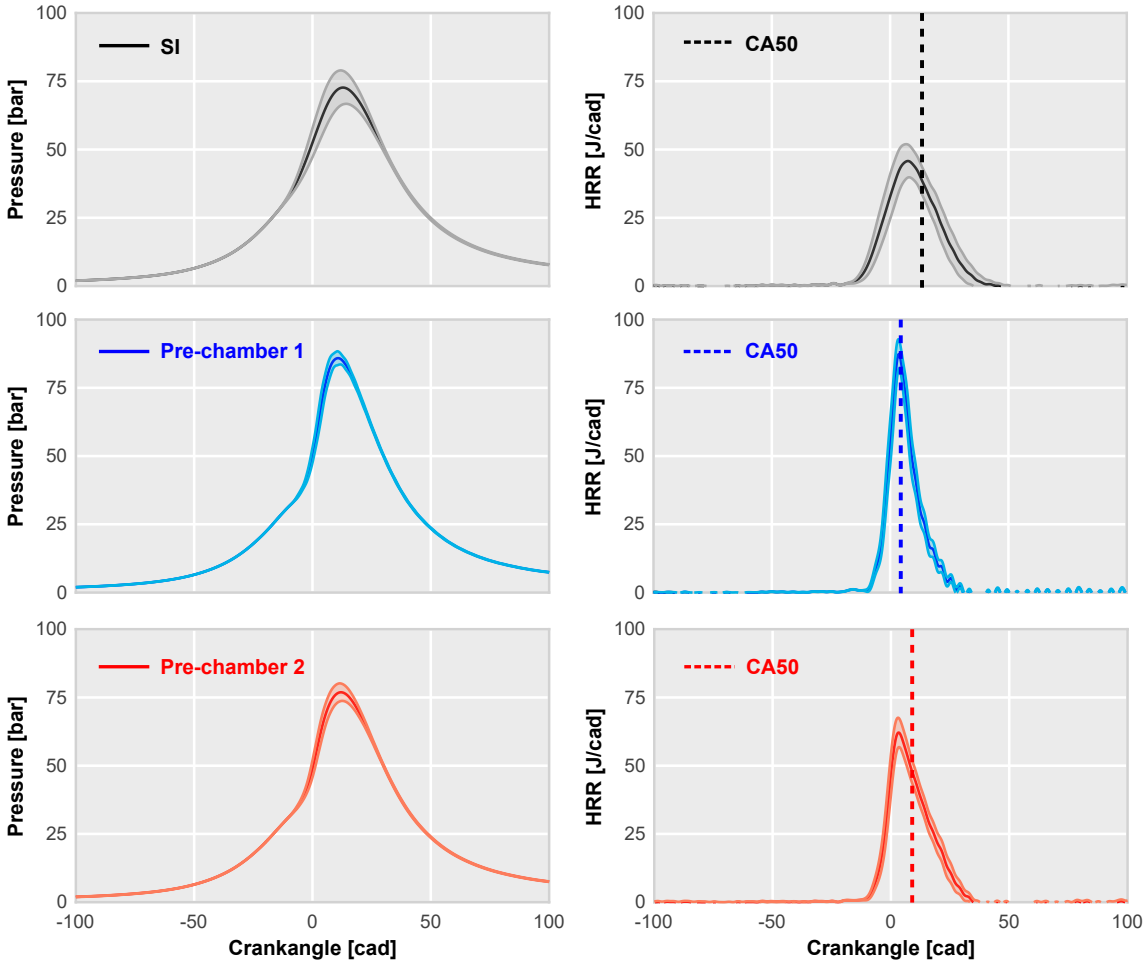

Figure 7: *In-cylinder pressure and rate of heat release at stoichiometric conditions with no EGR.*

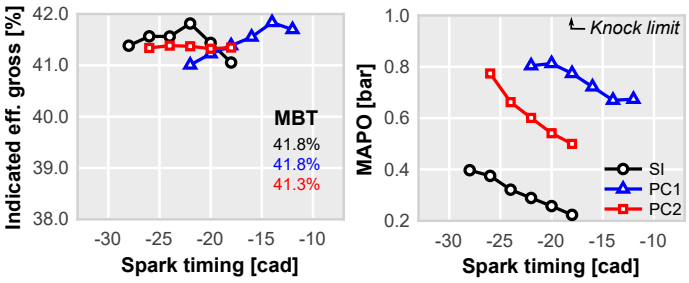

Figure 8: *Spark timing swept results at OP1. The gross indicated efficiency and knock intensity (MAPO) are plotted against the spark timing.*

indicated efficiency increases up to $\lambda = 1.5$, then drops below the conventional SI values. At this point, the number of misfiring cycles increase by 80% moving the COV of IMEP to unacceptable values. The huge increment of unburned hydrocarbons and CO in the exhaust is a consequence of the combustion stability worsening, causing a serious increase of misfiring cycles that eventually compromises efficiency. This can be easily seen in Fig. 10 where the in-cylinder pressure and HRR have been plotted for tests performed at the most extreme dilution conditions (after the maximum dilution ratio was achieved). The wide region of variability comes from complete misfiring to reasonable burning rate cycles.

Other relevant aspect observed form trends of Fig. 9, is the different tolerance to dilution obtained by the two pre-chambers under consideration. Directly comparing the peak dilution tests ($\lambda = 1.5$ for PC1 and $\lambda = 1.4$ for PC2), it can be observed a similar combustion stability (both efficiency and cycle-to-cycle variability) in both pre-chamber configurations. Therefore, differences in thermal efficiency are mostly caused by the improved combustion phasing (CA50) achieved by PC1. In addition, Since the gap between the maximum HRR is small, the local flow temperatures should be similar eventually resulting in comparable levels of NO_x.

In order to determine the possible causes for the different dilution tolerance, the 1D WAM model was employed for simulating the TJI tests at the maximum dilution ratio. Therefore, the PC1 design was simulated at 1.55 of λ and the PC2 at 1.45. The idea is to analyze which are the possible causes of this difference and to approve or refuse them in view of the measured results and the additional insight provided by the 1D model.

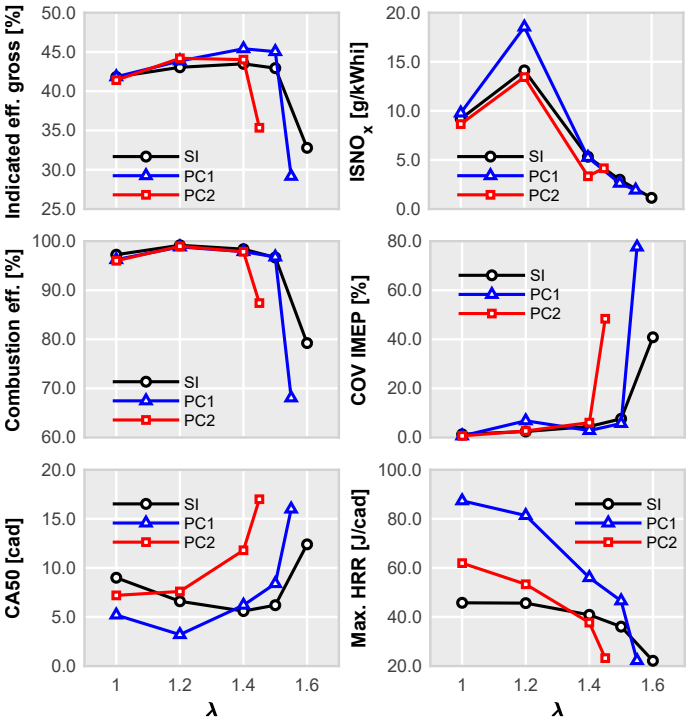

Figure 9: *Gross indicated efficiency, NO_x emissions, combustion efficiency, COV IMEP, combustion phasing and maximum HRR for air diluted conditions.*

Due to the distinct pre-chamber volumes, a possible explanation could be that the energy available for the main chamber ignition is not enough. Hence, an energy balance inside the pre-chamber during the ejection process was performed to compare the levels of energy available for igniting the main chamber.

During the ejection process, the total amount of energy is fixed by the amount of fuel within the pre-chamber at start of ejection. Note that the start of ejection may be varied depending on the spark timing used to achieve MBT. Thus, delaying the spark timing increases the available energy as the piston movement increases the mixture mass within the pre-chamber. This energy can be split in heat loss to the walls (Q_{wall}), unburned fuel inside the pre-chamber at the end of ejection process (Unburned), fuel mass loss through orifices due to the pressure increase (ejection in inert conditions, denoted as Inert) and the energy transferred to the jet (hereinafter refereed to as Energy Available for Ejection, EAE). The latter is the effective amount of energy available to generate the hot jet (in reacting conditions) and thus to ignite the main chamber.

Although all energy losses can be easily estimated using the 1D model outcomes, there are two main aspects to be taken into account when analyzing the results. On the one hand, the 1D model requires a combustion rate profile in both pre-chamber and main chamber due to the lack of a predictive combustion model. While the burning rate in the main chamber was obtained directly from the experiments through combustion diagnosis [43, 44], the combustion rate in the pre-chamber was calibrated to obtain a 99% of burned fuel at the end of ejection. Thereby, the amount of unburned fuel inside the pre-chamber at the end of ejection process (unburned) is low by definition. On the other hand, the 1D model assumes perfect mixing during combustion. This means that combustion products are being evacuated from the pre-chamber immediately after the combustion onset, minimizing the ejection of inert mixture (Inert).

More sophisticated numerical methods that consider geometrical effects (3D Computational Fluid Dynamics) revealed that both hypotheses are not as far as it might seem, especially considering that the electrodes are located at the top of the pre-chamber and the holes at the bottom. The small volume of the pre-chamber ensures that almost all mixture is consumed once the pressure in the main chamber inverts the flow among both chambers. Besides the proximity of the walls and the enhanced turbulence inside the pre-chamber distort the flame front while directing combustion products to a given hole by following a preferential path. In this sense, this process is somewhere in between perfect mixing and perfect scavenge. Therefore, assuming perfect mixing could be considered as the best possible situation, where the amount of flow ejected in inert conditions is minimum and it allows a qualitative analysis of the energy share available for igniting the main chamber.

Results of this study are shown in Table 6. Besides to the maximum dilution tests using both pre-chambers, stoichiometric tests are also included to quantify the reduction of available energy due to the spark timing advance as the dilution ratio increases and, the combustion duration is extended. The calculated values are normalized by their corresponding stoichiometric test. Inspecting these results, it is possible to verify that 'Unburned' and 'Inert' contributions are negligible due to the hypotheses described above. Moreover, the heat transfer to the walls (Q_{wall}) is also extremely low since the surface of the pre-chamber walls is small and the ejection process finishes in few milliseconds. Thus, the EAE is practically proportional to the total energy available within the pre-chamber at the spark timing.

Clear relationships can be found between the energy available inside the pre-chamber and the inception of the spark. As the piston pushes the gases into the pre-chamber, the amount of fuel increases. For instance, the total energy available inside PC1 decreases almost 40% when the spark timing is advanced from -18 (stoichiometric case) to -32 (maximum dilution case). Since the energy provided by any of both TJI configurations exceeds by far the energy provided by a conventional spark plug (70 mJ), it can be expected that the earlier ignition issues of passive pre-chamber concept are not due to the amount of energy available in the pre-chamber.

A second explanation could lie in the jets performance. Several authors [45, 46, 47, 48, 49, 50] investigated the effect of the jets features (penetration, entrainment, velocity...) on combustion. Hence, taking advantage of the 1D WAM model, a study of the jet dynamics was performed. First, the in-cylinder and pre-chamber pressure profiles are presented in Fig. 11 for analyzing the performance of the turbulent jets.

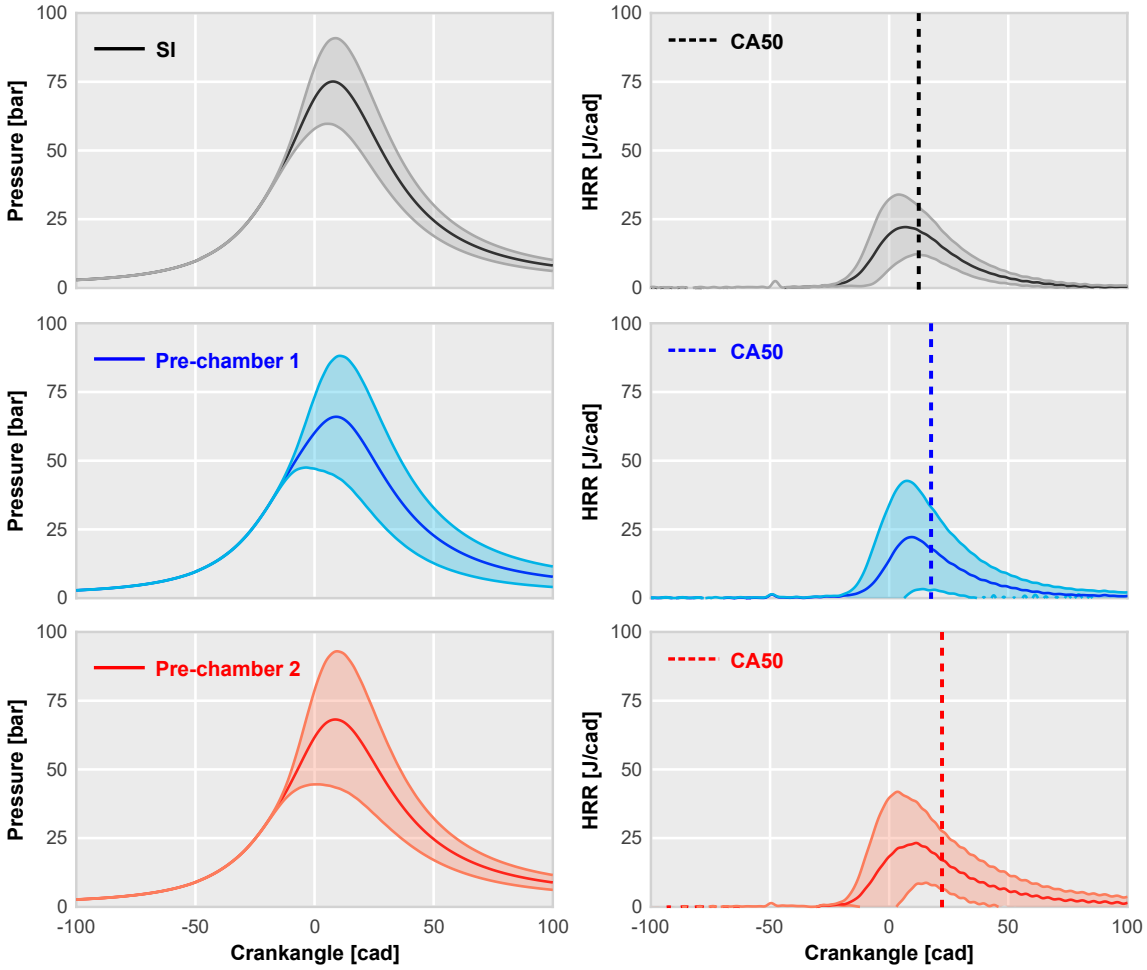

Figure 10: *In-cylinder pressure and heat release rate for the most extreme air dilution ratios measured.*

Table 6: *Energy balance inside the pre-chamber for PC1 and PC2 at high load/speed conditions.*

		EAE	Q_{wall}	Unburned	Inert	$\sum$
PC1	Stoich.	0.918	0.003	0.002	0.077	1.000
	Max. λ	0.585	0.002	0.003	0.000	0.590
PC2	Stoich.	0.950	0.005	0.000	0.045	1.000
	Max. λ	0.580	0.003	0.002	0.028	0.613

Here, the red profile, registered inside the pre-chamber unit, shows a secondary bump located around -25 CAD. This pressure perturbation is related to the PC combustion that forces the ejection of hot gas into the main chamber and its subsequent ignition. As it can be seen, there is no substantial differences among them and the maximum pressure difference between both chambers (Δp) is similar. These small differences are explained by the pre-chambers design itself (see Fig. 4 and Table 3), since they were designed to keep the same holes diameter and similar ratio between the total gas exchange area and the pre-chamber volume (PC1 = 3.9 m^{-1} and PC2 = 4.4 m^{-1}). As a result, the instantaneous velocity and mass flow rate trough a given orifice of the pre-chamber should be also similar. This is confirmed in Fig. 12 in which the temporal evolution of both parameters is plotted for the two PC configurations. The bulk temperature of the jets is also play a relevant role in the main chamber ignition. However, the variation of bulk temperature between both chambers is not representative, being around 2000 K in both cases.

In a conventional SI combustion, the rate of heat release depends on the flame propagation velocity, the amount of fuel per unit volume and the flame surface. Considering that the flame velocity and the density of the charge are similar at a given λ value (which are in fact reasonable hypotheses since the thermochemical properties are similar at a given engine load condition), a higher number of ignition locations increases the initial flame surface and therefore, higher HRR should be expected. This principle is being used in other ignition systems such as corona ignition [51], in which multiple electric arcs initiate the combustion process. The TJI concept also uses this principle in the main chamber: each turbulent jet ignites the main chamber charge at a given location, acting as a super-spark.

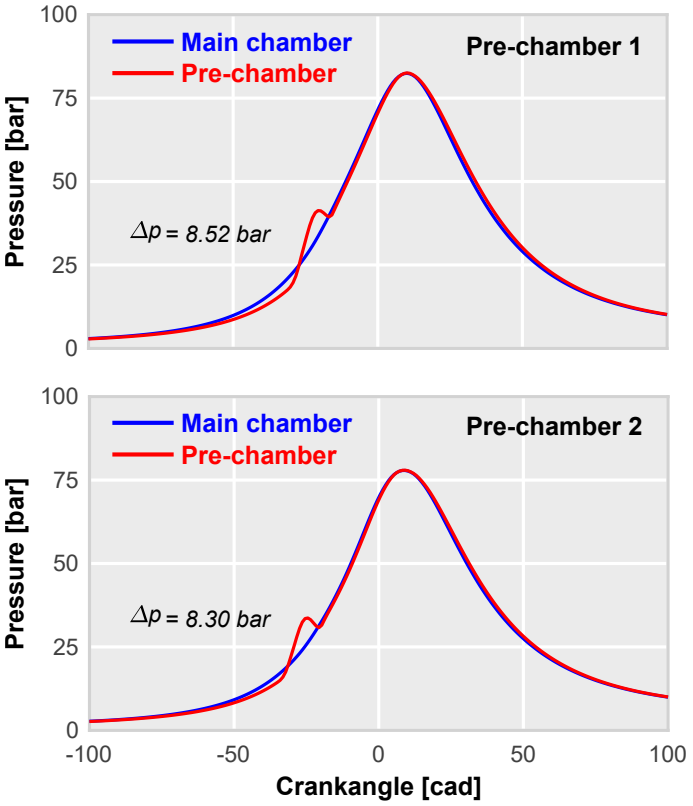

Figure 11: *Simulation of in-cylinder and pre-chamber pressures profiles for PC1 ($\lambda = 1.55$) and PC2 ($\lambda = 1.45$).*

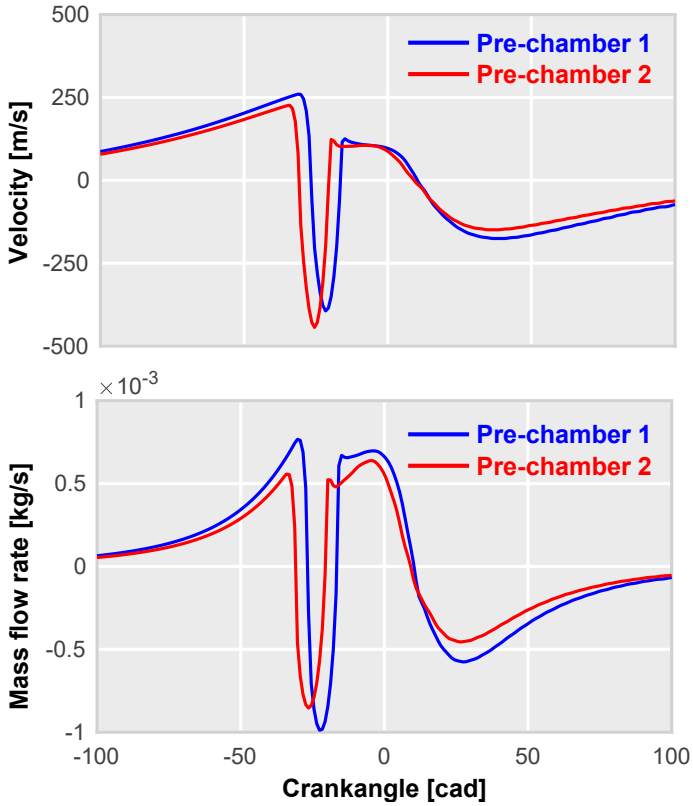

Figure 12: *Velocity and mass flow rate profiles for for PC1 ($\lambda = 1.55$) and PC2 ($\lambda = 1.45$).*

This trend is clearly observed in Fig. 9, the maximum HRR at $\lambda = 1$ increases with the number of the pre-chamber holes. Indeed, the ratio among PC1 and PC2 values is around 1.5 which coincides with the ratio of pre-chamber holes (6/4). Therefore, the relationship should be maintained throughout the whole dilution range if the root cause of the efficiency drop was conditioned only by the number of pre-chamber holes. However, this only happens with relatively low dilution ratios (from 0 to 40%), coinciding with the range where cycle-to-cycle dispersion is low. When CCV rises, the relationship is broken, being this cycle-to-cycle variability the main constraint to maintain, or even improve, efficiency levels at high dilution ratios (>50%).

It is therefore reasonable to conclude that the pre-chamber design is key aspect when optimizing the TJI concept for a particular condition of λ value. The internal fluid dynamics pattern of the pre-chamber must be smoothed to reduce the turbulence variability in the spark plug region, thereby decreasing CCV.

Recalling the trends observed in Fig. 9, it is also observed that the improvement in efficiency tends to be higher with the pre-chamber concept, especially with the PC1 configuration. As the bottom graphs of Fig. 9 show, this gain can be explained by the shortening of the combustion duration rather than by the combustion phasing. It should be noted that all test were performed at iso-fuel conditions thus, the higher maximum HRR, the shorter combustion. Lastly, NO_x emissions increase due to the increment of combustion rate and higher local temperatures achieved by the TJI combustion.

The other attractive strategy to improve efficiency while controlling NO_x emissions with the TWC, is the EGR dilution. The effects of increasing the the residual gas fraction in the intake are drawn in Fig. 13. Trends are very similar to those observed in the previous study. Both pre-chambers show competitive values of efficiency until the dilution limit is reached, then, an abrupt drop is accompanied by a worsening of the combustion stability. Again, this sharp decline is a consequence of the considerable increase of misfiring cycles. However, the tolerance to dilution with EGR is lower than with air. If we compare the maximum dilution ratio of PC1, it is around 55% when diluting with air (see Fig. 9) but around 15% when using EGR (see Fig. 13). This suggests that the optimum pre-chamber design for operating with air dilution, may not be adequate for the EGR-diluted operation.

In contrast to what we observed when increasing the air-to-fuel ratio, this strategy (a combination of TJI and EGR dilution) is not able to improve the efficiency levels achieved by the conventional SI. Regarding pollutant emissions, NO_x levels decreases with the increment of the dilution ratio. Nevertheless, differences between all concepts are less apparent.

To end the study of the dilution impact, the last step is to contrast the measured trends using CNG and gasoline fuel. This is particularly interesting since the pre-chambers con-

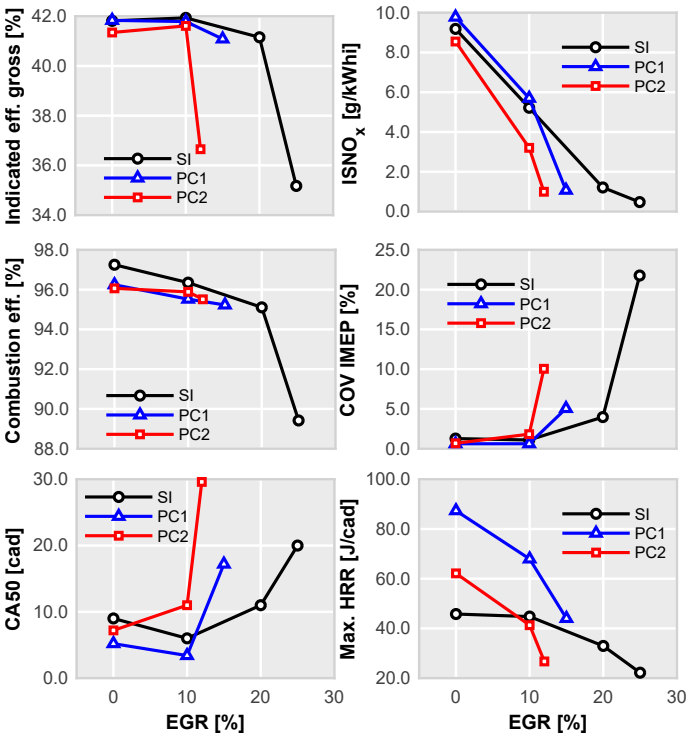

Figure 13: *Gross indicated efficiency, NO_x emissions, combustion efficiency, COV IMEP, combustion phasing and maximum HRR for EGR diluted conditions.*

figuration was originally developed to operate with gasoline fuel. Results published in [24] show that the maximum dilution ratio is 60% with air and 20% with EGR for the same PC1 configuration and gasoline fuel. In both cases, the tolerance to dilution has been reduced 5%, evincing that fuel properties are also determinant in the pre-chamber design optimization. Thus, the uniformity of the flow field (local velocity fluctuations) and the turbulence length must be adapted to the physical and chemical properties of the fuel.

4.4. Operation at low engine load and speed conditions

The experimental campaign was concluded with a spark timing swept at low engine speed and load conditions. General trends of these tests are shown in Fig. 14. Particularly, the gross indicated efficiency, NO_x emissions, exhaust temperature, combustion stability, phasing and velocity were selected to display the strengths and weaknesses of the concept. The indicated efficiency gap between conventional SI and TJI is significantly larger. The characteristic combustion shortening of TJI leads to a higher relative heat loss that notably compromises the efficiency levels at this engine speed.

The combustion stability progressively decreases as the combustion is moved towards the expansion stroke in the conventional SI concept whereas it is suddenly compromised at a given ST in the pre-chamber ignition concept. This behavior is specifically critical in the PC2 configuration, where the effective operating range is extremely narrow and two crank angle degree of ST variation entails almost 2% of efficiency loss.

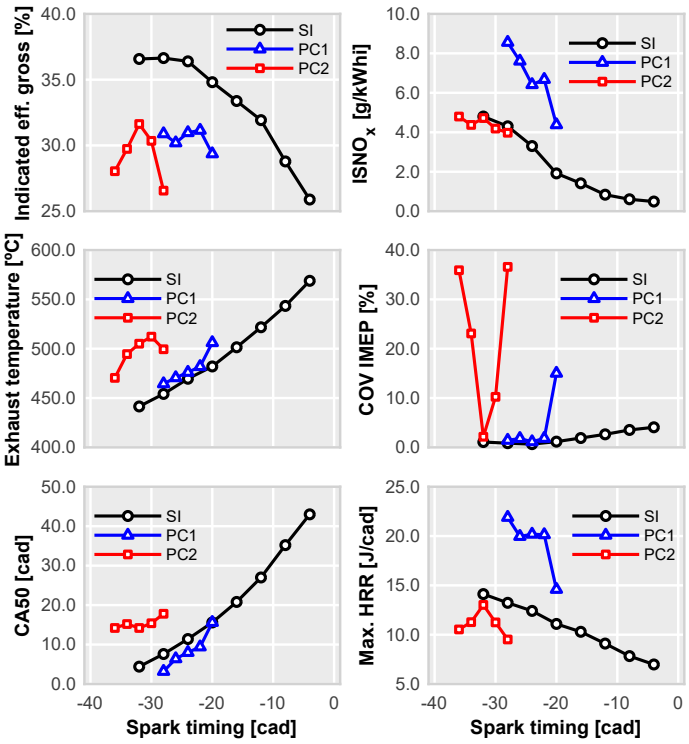

Figure 14: *Gross indicated efficiency, NO_x emissions, exhaust temperature, COV IMEP, combustion phasing and combustion velocity for the spark timing swept.*

As in the previous section, the energy balance inside the pre-chamber is performed to dig into the root cause of the limited operating range of the PC2 configuration. Results presented in Table 7 show a comparison between PC1 and PC2 of the energy available within the PC and its distribution. Here, results are normalized by the values of PC1 test. The available energy for the jets generation is considerably higher for PC1 than for PC2 (≈70%), mainly due to the difference in volume. As PC1 is larger, it is capable to store higher amount of fuel during the pre-chamber filling, leading to an increased potential to generate suitable jets. Therefore, the lack of performance shown by the PC2 configuration can be partially explained by the low capability to store energy and use it properly to ignite the main chamber.

Table 7: *Energy balance inside the pre-chamber for PC1 and PC2 at low load/speed conditions.*

	EAE	Q_{wall}	Unburned	Inert	$\sum$
PC1	0.714	0.003	0.010	0.273	1.000
PC2	0.408	0.003	0.007	0.172	0.590

In view of the relevance of the energy available inside the pre-chamber, the energy balance inside the pre-chamber for the two operating points considered so far is presented in Table 8. In this table, the energy values are normalized

to the PC1 test of each operating condition. It can be seen that the difference in the pre-chamber volume affects the EAE in PC2 at any operating condition, reducing its potential to generate suitable reacting jets. Furthermore, the loss of fuel mass in inert conditions decreases with engine speed since the duration of the ejection process is reduced.

In order to provide a complete overview of the energy share trends, the results obtained for the same study are normalized to the available energy in the PC1 at OP1 test and presented in Table 9. Results show a clear relationship between the engine load and the energy available for igniting the main chamber (EAE). This energy decreases drastically at low load conditions (OP2), specially in the PC2 configuration. PC1 configuration is able to maintain a suitable energy share in all operating conditions, assuring a stable operation over the whole operating range. By contrast, PC2 fails to maintain reasonable values of EAE share at low load conditions.

Table 8: *Energy balance inside the pre-chamber for PC1 and PC2 of the two operating points.*

		EAE	Q_{wall}	Unburned	Inert	$\sum$
OP1	PC1	0.918	0.003	0.002	0.077	1.000
	PC2	0.491	0.003	0.000	0.023	0.517
OP2	PC1	0.714	0.003	0.010	0.273	1.000
	PC2	0.408	0.003	0.007	0.172	0.590

Table 9: *Energy balance inside the pre-chamber for PC1 and PC2 of the two operating points.*

		EAE	Q_{wall}	Unburned	Inert	$\sum$
PC1	OP1	0.918	0.003	0.002	0.077	1.000
	OP2	0.271	0.001	0.004	0.103	0.379
PC2	OP1	0.491	0.003	0.000	0.023	0.517
	OP2	0.155	0.001	0.003	0.066	0.225

4.4.1. Compatibility with aftertreatment strategies

Based on the previous knowledge [52], there are two potential solutions to increase the flow temperature at the exhaust tailpipe. The addition of EGR has the effect of increasing the combustion duration, which turns into a higher exhaust temperature as the combustion process extends towards the Exhaust Valves Opening (EVO). The second attempt consisted of increasing the intake temperature in order to rise the global trapped gas temperature along the closed cycle and, subsequently, the temperature at the exhaust pipe.

Therefore, the next step in the experimental campaign was to perform different EGR dilution and intake temperature sweeps at low load/speed conditions. Since the suitable operation of PC2 is compromised even at non-diluted conditions, it was deemed necessary to exclude this pre-chamber design for the upcoming tests.

The effect of adding EGR is presented in Fig. 15. In this study, conventional SI and TJI PC1 configurations have been tested, increasing the EGR dilution at 5% and 10% while sweeping the spark timing until the measurements were compromised by the combustion instability. Results show an increment of the exhaust temperature as the dilution ratio is increased for both SI and TJI concepts. Despite the effective ST range is still very constrained when operating with the TJI concept, the impact of the EGR on the exhaust temperature is higher. Note that the gap between blue (TJI) lines is larger than black ones (SI). In both cases, combustion is shifted towards the expansion stroke with the increment of the EGR rate, increasing the in-cylinder temperature at EVO. Thereby, the exhaust temperature increases 50ºC when switching from non-diluted conditions to 10% of EGR rate.

The interest of this strategy lies in the efficiency trends observed. Increasing the EGR rate reduces the pumping losses, thereby maintaining the gross indicated efficiency at competitive values even with a extreme delayed combustion (CA50 $>$ 30 cad). Since the use of EGR does not penalize the fuel consumption, it appears as a very interesting strategy to increase the exhaust temperature and to activate the TWC. Nevertheless, it is true that the exhaust temperatures attainable with the TJI concept are not comparable with those achieved by the conventional SI concept (50ºC of difference) due to the limited ST timing range.

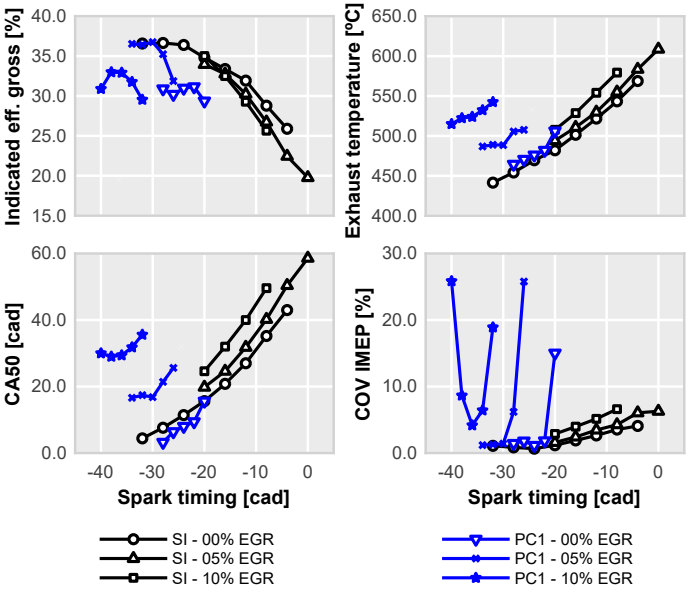

Figure 15: *Comparison of gross indicated efficiency, exhaust temperature, COV IMEP and combustion phasing and for the spark timing and EGR dilution swept.*

Results of the second potential strategy are shown in Fig. 16. Here, the intake temperature was increased from 30ºC to 70ºC in both considered SI and TJI configurations. Trends are similar to those observed in the previous study, increasing the flow temperature helps to slightly rise the exhaust temperature but the narrow ST timing range limits its maximum attainable value. On the contrary, the increase of the pump-

ing losses results in a significant efficiency loss that makes this strategy less attractive from the point of view of fuel consumption.

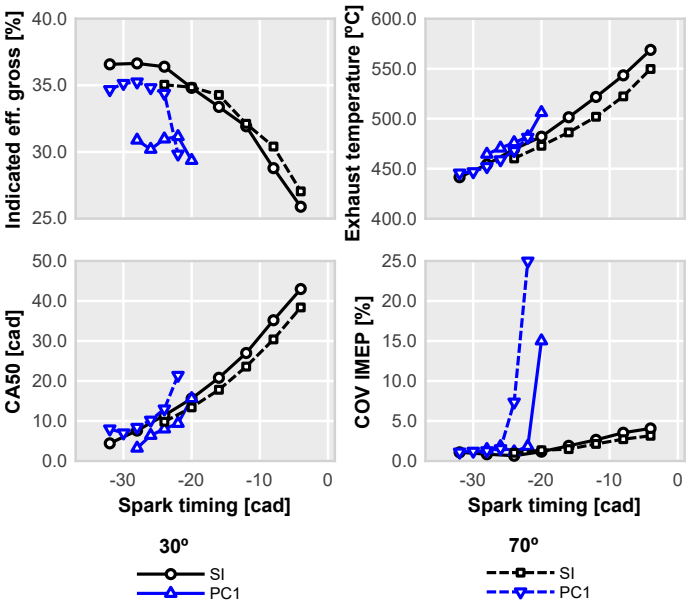

Figure 16: *Comparison of gross indicated efficiency, exhaust temperature, COV IMEP and combustion phasing and for the spark timing and increased intake temperature swept.*

5. Summary and conclusions

The potential advantages of using natural gas in automotive power-plants have been evaluated. In particular, the passive pre-chamber ignition concept fueled by compressed natural gas has been studied in a turbo-charged high-compression ratio spark-ignition engine. The main conclusions of the study are summarized here:

- Combustion of compressed natural gas refined by different renewable sources not only reduces the global GHG emission but also may contribute to remove the existent pollution. The life cycle of this fuel is significantly lower that traditional gasoline-based fuels even considering the worst strategy for production, transportation and compression.
- This technology does not allow to extend the maximum dilution limit beyond the limits achieved by conventional SI combustion. This is mainly due two reasons: the low laminar flame speed of the compressed natural gas and the internal fluid dynamics of the pre-chamber.
- The TJI concept is more tolerant to air dilution. The maximum air dilution ratio archived with this configuration is close to 50% while it is around 15% for residual exhaust gases, being clearly insufficient to avoid the use of the TWC to fulfill the current and future emission levels established by public institutions.
- The combustion phasing can be moved freely to reach MBT conditions without any remarkable restriction since thermochemical properties of natural gas prevent knocking combustion. In these conditions the gains in efficiency are negligible when switching from SI to TJI.
- The operation at low load and engine speed seems to be the main constraint of this ignition system. The increased heat loss due to the shorter combustion process worsens the efficiency levels. This efficiency loss is around 5% if it is compared with the conventional SI combustion. Besides, decreasing the pre-chamber volume can make this situation even worse. In addition, the TJI concept show notably lower flow temperature at the exhaust manifold hindering the activation of the three-way catalyst.
- Although a substantial increment of exhaust temperature (around 50ºC) has been found when increasing the EGR rate up to 10%, the deterioration of the combustion stability impedes to reach the values measured with conventional SI combustion. Increasing the intake flow temperature only showed a marginal improvement of the exhaust temperature with a significant efficiency loss.
- Other side issues, such as those related to the different air-to-fuel ratio and LHV, are also relevant especially when contrasting the impact of different fuels in the same power-plant. Nevertheless, the improved knock resistance reveal a room for efficiency improvements.

After the analysis of the results, a clear room for improvement can be observed. New paths to explore the concept capabilities in the search of a fully sustainable global transport can be easily identified. For example, combining this engine platform with a increased compression ratio and/or other combustion strategies based on dual fuel blends (i.e. CNG + H_2) could open a new way to find higher thermal efficiency, while decreasing the tank-to-wheel emissions.

Acknowledgements

The work has been partially supported by the Spanish Ministerio de Economía y Competitividad through grant number TRA2017-89139-C2-1-R.

P. J. Martinez-Hernandiz is partially supported by an FPI contract (FPI-S2-19-21993) of the "Programa de Apoyo para la Investigación y Desarrollo (PAID-05-19)" of the Universitat Politècnica de València.

The authors want to express their gratitude to CONVERGENT SCIENCE Inc. and Convergent Science GmbH for their kind support for the 0D and 1D calculations with the CONVERGE software.

The authors also wish to thank Mr. Gabriel Alcantarilla for his inestimable assistance during the experimental campaign.

[1] M. Ruiz-Medina, R. Espejo, Integration of spatial functional interaction in the extrapolation of ocean surface temperature anomalies due to global warming, International Journal of Applied Earth Observation and Geoinformation 22 (2013) 27 – 39, spatial Statistics for Mapping the Environment. doi:https://doi.org/10.1016/j.jag.2012.01.021.
URL http://www.sciencedirect.com/science/article/pii/S0303243412000232

[2] G. Walden, C. Noirot, I. Nagelkerken, A future 1.2 °c increase in ocean temperature alters the quality of mangrove habitats for marine plants and animals, Science of The Total Environment 690 (2019) 596 – 603. doi:https://doi.org/10.1016/j.scitotenv.2019.07.029.
URL http://www.sciencedirect.com/science/article/pii/S0048969719331420

[3] D. Easterbrook, Chapter 9 - greenhouse gases, in: D. J. Easterbrook (Ed.), Evidence-Based Climate Science (Second Edition), second edition Edition, Elsevier, 2016, pp. 163 – 173. doi:https://doi.org/10.1016/B978-0-12-804588-6.00009-4.
URL http://www.sciencedirect.com/science/article/pii/B9780128045886000094

[4] M. Hoogwijk, A. Faaij, B. Eickhout, B. de Vries, W. Turkenburg, Potential of biomass energy out to 2100, for four ipcc sres land-use scenarios, Biomass and Bioenergy 29 (4) (2005) 225 – 257. doi:https://doi.org/10.1016/j.biombioe.2005.05.002.
URL http://www.sciencedirect.com/science/article/pii/S0961953405000759

[5] S. Harris, J. Weinzettel, A. Bigano, A. Källmén, Low carbon cities in 2050? ghg emissions of european cities using production-based and consumption-based emission accounting methods, Journal of Cleaner Production 248 (2020) 119206. doi:https://doi.org/10.1016/j.jclepro.2019.119206.
URL http://www.sciencedirect.com/science/article/pii/S0959652619340764

[6] G. Pleßmann, P. Blechinger, How to meet eu ghg emission reduction targets? a model based decarbonization pathway for europe's electricity supply system until 2050, Energy Strategy Reviews 15 (2017) 19 – 32. doi:https://doi.org/10.1016/j.esr.2016.11.003.
URL http://www.sciencedirect.com/science/article/pii/S2211467X16300530

[7] Z. Ran, D. Hariharan, B. Lawler, S. Mamalis, Exploring the potential of ethanol, cng, and syngas as fuels for lean spark-ignition combustion-an experimental study, Energy 191 (2020) 116520.

[8] J. Lee, C. Park, J. Bae, Y. Kim, S. Lee, C. Kim, Comparison between gasoline direct injection and compressed natural gas port fuel injection under maximum load condition, Energy 197 (2020) 117173.

[9] O. Hijazi, S. Munro, B. Zerhusen, M. Effenberger, Review of life cycle assessment for biogas production in europe, Renewable and Sustainable Energy Reviews 54 (2016) 1291 – 1300. doi:https://doi.org/10.1016/j.rser.2015.10.013.
URL http://www.sciencedirect.com/science/article/pii/S1364032115010928

[10] N. Scarlat, J.-F. Dallemand, F. Fahl, Biogas: Developments and perspectives in europe, Renewable Energy 129 (2018) 457 – 472. doi:https://doi.org/10.1016/j.renene.2018.03.006.
URL http://www.sciencedirect.com/science/article/pii/S096014811830301X

[11] K. Hartley, R. van Santen, J. Kirchherr, Policies for transitioning towards a circular economy: Expectations from the european union (eu), Resources, Conservation and Recycling 155 (2020) 104634. doi:https://doi.org/10.1016/j.resconrec.2019.104634.
URL http://www.sciencedirect.com/science/article/pii/S0921344919305403

[12] Y. Karagöz, Analysis of the impact of gasoline, biogas and biogas + hydrogen fuels on emissions and vehicle performance in the wltc and nedc, International Journal of Hydrogen Energy 44 (59) (2019) 31621 – 31632. doi:https://doi.org/10.1016/j.ijhydene.2019.10.019.
URL http://www.sciencedirect.com/science/article/pii/S0360319919337589

[13] G. J. Germane, C. G. Wood, C. C. Hess, Lean combustion in spark-ignited internal combustion engines - a review, in: 1983 SAE International Fall Fuels and Lubricants Meeting and Exhibition, SAE International, 1983. doi:https://doi.org/10.4271/831694.
URL https://doi.org/10.4271/831694

[14] W. P. Attard, H. Blaxill, A lean burn gasoline fueled pre-chamber jet ignition combustion system achieving high efficiency and low nox at part load, in: SAE 2012 World Congress & Exhibition, SAE International, 2012. doi:https://doi.org/10.4271/2012-01-1146.
URL https://doi.org/10.4271/2012-01-1146

[15] F. A. Ayala, Combustion lean limits fundamentals and their application to a si hydrogen-enhanced engine concept, Ph.D. thesis, Massachusetts Institute of Technology (2006).

[16] F. A. Ayala, M. D. Gerty, J. B. Heywood, Effects of combustion phasing, relative air-fuel ratio, compression ratio, and load on si engine efficiency, in: SAE 2006 World Congress & Exhibition, SAE International, 2006. doi:https://doi.org/10.4271/2006-01-0229.
URL https://doi.org/10.4271/2006-01-0229

[17] F. A. Ayala, J. B. Heywood, Lean si engines: The role of combustion variability in defining lean limits, in: 8th International Conference on Engines for Automobiles, Consiglio Nazionale delle Ricerche, 2007. doi:https://doi.org/10.4271/2007-24-0030.
URL https://doi.org/10.4271/2007-24-0030

[18] J. Dale, M. Checkel, P. Smy, Application of high energy ignition systems to engines, Progress in Energy and Combustion Science 23 (5) (1997) 379 – 398. doi:https://doi.org/10.1016/S0360-1285(97)00011-7.
URL http://www.sciencedirect.com/science/article/pii/S0360128597000117

[19] M. Zheng, S. Yu, Advanced ignition systems for future clean combustion engines: Review, Journal of Automotive Saftey and Engery 6 (4) (2015) 295–313.

[20] W. P. Attard, N. Fraser, P. Parsons, E. Toulson, A turbulent jet ignition pre-chamber combustion system for large fuel economy improvements in a modern vehicle powertrain, SAE International Journal of Engines 3 (2) (2010) 20–37. doi:https://doi.org/10.4271/2010-01-1457.
URL https://doi.org/10.4271/2010-01-1457

[21] N. D. S. A. Santos, C. E. C. Alvarez, V. R. Roso, J. G. C. Baeta, R. M. Valle, Combustion analysis of a si engine with stratified and homogeneous pre-chamber ignition system using ethanol and hydrogen, Applied Thermal Engineering 160 (2019) 113985. doi:https://doi.org/10.1016/j.applthermaleng.2019.113985.
URL http://www.sciencedirect.com/science/article/pii/S1359431119316151

[22] W. P. Attard, J. Kohn, P. Parsons, Ignition energy development for a spark initiated combustion system capable of high load, high efficiency and near zero nox emissions, SAE International Journal of Engines 3 (2) (2010) 481–496. doi:https://doi.org/10.4271/2010-32-0088.
URL https://doi.org/10.4271/2010-32-0088

[23] L. S. Baumgartner, S. Wohlgemuth, S. Zirngibl, G. Wachtmeister, Investigation of a methane scavenged prechamber for increased efficiency of a lean-burn natural gas engine for automotive applications, SAE International Journal of Engines 8 (2) (2015) 921–933.
URL http://www.jstor.org/stable/26277994

[24] J. Benajes, R. Novella, J. Gomez-Soriano, P. Martinez-Hernandiz, C. Libert, M. Dabiri, Evaluation of the passive pre-chamber ignition concept for future high compression ratio turbocharged spark-ignition engines, Applied Energy 248 (2019) 576 – 588. doi:https://doi.org/10.1016/j.apenergy.2019.04.131.
URL http://www.sciencedirect.com/science/article/pii/S030626191930769X

[25] E. Mastorakos, P. Allison, A. Giusti, P. De Oliveira, S. Benekos, Y. Wright, C. Frouzakis, K. Boulouchos, Fundamental aspects of jet ignition for natural gas engines, JSTOR, 2017. doi:https://doi.org/10.4271/2017-24-0097.
URL https://doi.org/10.4271/2017-24-0097

[26] S. Heyne, M. Meier, B. Imbert, D. Favrat, Experimental investigation of prechamber autoignition in a natural gas engine for cogeneration, Fuel 88 (3) (2009) 547 – 552. doi:https:

//doi.org/10.1016/j.fuel.2008.09.032.
URL http://www.sciencedirect.com/science/article/pii/S0016236108003712

[27] R. Ślefarski, M. Gołębiewski, P. Czyżewski, P. Grzymisławski, J. Wawrzyniak, Analysis of combustion process in industrial gas engine with prechamber-based ignition system, Energies 11 (2). doi:https://doi.org/10.3390/en11020336.
URL https://www.mdpi.com/1996-1073/11/2/336

[28] A. Jamrozik, Lean combustion by a pre-chamber charge stratification in a stationary spark ignited engine, Journal of Mechanical Science and Technology 29 (5) (2015) 2269–2278. doi:https://doi.org/10.1007/s12206-015-0145-7.

[29] Z. Chen, Y. Ai, T. Qin, F. Luo, Quantitative evaluation of n-butane concentration on knock severity of a natural gas heavy-duty si engine, Energy 189 (2019) 116244.

[30] A. Shah, P. Tunestal, B. Johansson, Investigation of performance and emission characteristics of a heavy duty natural gas engine operated with pre-chamber spark plug and dilution with excess air and egr, SAE International Journal of Engines 5 (4) (2012) 1790–1801.
URL http://www.jstor.org/stable/26277581

[31] B. Korb, K. Kuppa, H. D. Nguyen, F. Dinkelacker, G. Wachtmeister, Experimental and numerical investigations of charge motion and combustion in lean-burn natural gas engines, Combustion and Flame 212 (2020) 309 – 322. doi:https://doi.org/10.1016/j.combustflame.2019.11.005.
URL http://www.sciencedirect.com/science/article/pii/S0010218019305024

[32] C. Park, C. Kim, S. Lee, S. Lee, J. Lee, Comparative evaluation of performance and emissions of cng engine for heavy-duty vehicles fueled with various caloric natural gases, Energy 174 (2019) 1–9.

[33] B. Najafi, E. Akbarian, S. M. Lashkarpour, M. Aghbashlo, H. S. Ghaziaskar, M. Tabatabaei, Modeling of a dual fueled diesel engine operated by a novel fuel containing glycerol triacetate additive and biodiesel using artificial neural network tuned by genetic algorithm to reduce engine emissions, Energy 168 (2019) 1128–1137.

[34] J. M. Luján, H. Climent, R. Novella, M. E. Rivas-Perea, Influence of a low pressure egr loop on a gasoline turbocharged direct injection engine, Applied Thermal Engineering 89 (2015) 432 – 443. doi:https://doi.org/10.1016/j.applthermaleng.2015.06.039.
URL http://www.sciencedirect.com/science/article/pii/S1359431115005931

[35] M. Sens, E. Binder, Pre-chamber ignition as a key technology for future powertrain fleets, MTZ worldwide 80 (2) (2019) 44–51. doi:10.1007/s38313-018-0150-1.
URL https://doi.org/10.1007/s38313-018-0150-1

[36] V. R. Roso, N. D. S. A. Santos, R. M. Valle, C. E. C. Alvarez, J. Monsalve-Serrano, A. García, Evaluation of a stratified prechamber ignition concept for vehicular applications in real world and standardized driving cycles, Applied Energy 254 (2019) 113691. doi:https://doi.org/10.1016/j.apenergy.2019.113691.
URL http://www.sciencedirect.com/science/article/pii/S0306261919313789

[37] J. Benajes, R. Novella, J. Gomez-Soriano, P. Martinez-Hernandiz, C. Libert, M. Dabiri, Performance of the passive pre-chamber ignition concept in a spark-ignition engine for passenger car applications, in: SIA Powertrain & Electronics, 2019.

[38] CONVERGENT SCIENCE Inc., CONVERGE 2.3 Theory Manual (2017).

[39] G. Vanhove, G. Petit, R. Minetti, Experimental study of the kinetic interactions in the low-temperature autoignition of hydrocarbon binary mixtures and a surrogate fuel, Combustion and Flame 145 (3) (2006) 521 – 532. doi:https://doi.org/10.1016/j.combustflame.2006.01.001.
URL http://www.sciencedirect.com/science/article/pii/S0010218006000277

[40] R. Minetti, M. Carlier, M. Ribaucour, E. Therssen, L. Sochet, Comparison of oxidation and autoignition of the two primary reference fuels by rapid compression, Symposium (International) on Combustion 26 (1) (1996) 747 – 753. doi:https://doi.org/10.1016/S0082-0784(96)80283-9.
URL http://www.sciencedirect.com/science/article/pii/S0082078496802839

[41] A. Burnham, M. Wang, Y. Wu, Development and applications of greet 2.7–the transportation vehicle-cyclemodel., Tech. rep., Argonne National Lab.(ANL), Argonne, IL (United States) (2006).

[42] S. Fuss, J. G. Canadell, G. P. Peters, M. Tavoni, R. M. Andrew, P. Ciais, R. B. Jackson, C. D. Jones, F. Kraxner, N. Nakicenovic, et al., Betting on negative emissions, Nature climate change 4 (10) (2014) 850–853.

[43] M. Lapuerta, O. Armas, J. Hernández, Diagnosis of di diesel combustion from in-cylinder pressure signal by estimation of mean thermodynamic properties of the gas, Applied Thermal Engineering 19 (5) (1999) 513 – 529. doi:https://doi.org/10.1016/S1359-4311(98)00075-1.
URL http://www.sciencedirect.com/science/article/pii/S1359431198000751

[44] F. Payri, S. Molina, J. Martín, O. Armas, Influence of measurement errors and estimated parameters on combustion diagnosis, Applied Thermal Engineering 26 (2) (2006) 226 – 236. doi:https://doi.org/10.1016/j.applthermaleng.2005.05.006.
URL http://www.sciencedirect.com/science/article/pii/S1359431105001560

[45] G. Xu, M. Kotzagianni, P. Kyrtatos, Y. M. Wright, K. Boulouchos, Experimental and numerical investigations of the unscavenged prechamber combustion in a rapid compression and expansion machine under engine-like conditions, Combustion and Flame 204 (2019) 68 – 84. doi:https://doi.org/10.1016/j.combustflame.2019.01.025.
URL http://www.sciencedirect.com/science/article/pii/S0010218019300434

[46] E. Toulson, H. C. Watson, W. P. Attard, Modeling alternative prechamber fuels in jet assisted ignition of gasoline and lpg, in: SAE World Congress & Exhibition, SAE International, 2009. doi:https://doi.org/10.4271/2009-01-0721.
URL https://doi.org/10.4271/2009-01-0721

[47] S. Biswas, S. Tanvir, H. Wang, L. Qiao, On ignition mechanisms of premixed ch4/air and h2/air using a hot turbulent jet generated by pre-chamber combustion, Applied Thermal Engineering 106 (2016) 925 – 937. doi:https://doi.org/10.1016/j.applthermaleng.2016.06.070.
URL http://www.sciencedirect.com/science/article/pii/S135943111630984X

[48] M. Muller, C. Freeman, P. Zhao, H. Ge, Numerical simulation of ignition mechanism in the main chamber of turbulent jet ignition system, ASME 2018 Internal Combustion Engine Division Fall Technical Conference.

[49] J. M. Desantes, R. Novella, J. De La Morena, et al., Achieving ultra-lean combustion using a pre-chamber spark ignition system in a rapid compression-expansion machine, SAE Technical Paper.

[50] B. C. Thelen, G. Gentz, E. Toulson, Computational study of a turbulent jet ignition system for lean burn operation in a rapid compression machine, in: SAE 2015 World Congress & Exhibition, SAE International, 2015. doi:https://doi.org/10.4271/2015-01-0396.
URL https://doi.org/10.4271/2015-01-0396

[51] V. Heise, P. Farah, H. Husted, E. Wolf, High frequency ignition system for gasoline direct injection engines, SAE Technical Paper.

[52] H. Wei, T. Zhu, G. Shu, L. Tan, Y. Wang, Gasoline engine exhaust gas recirculation – a review, Applied Energy 99 (2012) 534 – 544. doi:https://doi.org/10.1016/j.apenergy.2012.05.011.
URL http://www.sciencedirect.com/science/article/pii/S0306261912003595

Nomenclature

A/F_{st}	Air-to-fuel stoichiometric ratio	—
AID	Auto-ignition delay	ms
BC	Black carbon	kg/MJ
CA50	Crank angle at which combustion reaches 50%	cad
CCV	Cycle to cycle variability	—
CFD	Computational fluid dynamics	—
CH_4	Methane	kg/MJ
CNG	Compressed natural gas	—
CO	Carbon monoxide	kg/MJ
CO_2	Carbon dioxide	kg/MJ
COV	Coefficient of variation	%
CD	Combustion duration	cad
Δp	Difference between pre and main chamber pressure	bar
DOHC	Double-overhead camshaft	—
EAE	Energy available for ejection	J
EGR	External gases recirculation	%
EV	Electric vehicle	—
EVO	Exhaust valves opening	cad
FSN	Filter smoke number	—
FW	Food waste	—
GHG	Green house gases	kg/MJ
HRR	Heat release rate	J/cad
ICE	Internal combustion engine	—
IMEP	Indicated mean effective pressure	bar
λ	Air-to-fuel ratio	—
LCA	Life cycle analysis	—
LG	Landfill gas	—
LHV	Lower heating value	MJ/kg
MAPO	Maximum amplitude pressure oscillation	bar
MBT	Maximum brake torque	—
N_2O	Nitrous oxide	kg/MJ
NG	Natural gas	—
NO_x	Nitrogen oxides	kg/MJ
NTC	Negative temperature coefficient	—
O_2	Oxigen	kg/MJ
OP	Operating point	—
PC	Pre-chamber	—
PFI	Port fuel injection	—
PM	Particulate matter	kg/MJ
POC	Pollutants of concern	kg/MJ
RON	Research octane number	—
SI	Spark ignition	—
SOE	Start of ejection	—
SO_x	Sulfur oxides	kg/MJ
ST	Spark timing	cad
τ	Auto-ignition delay time	ms
TDC	Top dead center	—
TJI	Turbulent jet ignition	—
TWC	Three-way catalyst	—
VOC	Volatil organic pound	kg/MJ
WAM	Wave action model	—
WS	Waste sludge	kg/MJ